Axial Impact Behavior and Energy Absorption of Rubberized Concrete with/without FRP Confinement

Thong M. Pham[1], Mohamed Elchalakani[2], Ali Karrech[3] and Hong Hao[4]

Abstract

This study investigates the axial impact resistance and energy absorption of rubberized concrete with/without fiber reinforced polymer (FRP) confinement. The impact tests were carried out by using an instrumented drop-weight testing apparatus. The experimental results have shown that rubberized concrete significantly reduced the maximum impact force of up to 50% and extended the impact duration. These characteristics make rubberized concrete a promising material for protective structures and particularly for future sustainable construction of rigid roadside barriers. Glass FRP confinement is a very effective method to improve the impact resistance for both conventional concrete and particularly for rubberized concrete. It was found that the rubberized concrete reduced the maximum impact force so that it transferred a lower force to a protected structure as well as a lower rebound force, which is desirable for protection of passengers in a an incident of vehicle collision. Interestingly, the rubberized concrete showed a lower energy absorption capacity as compared to conventional concrete, where the exact reason for this is unknown to the authors. Therefore, further research is sought to provide more

[1] Research Fellow, Center for Infrastructural Monitoring and Protection, School of Civil and Mechanical Engineering, Curtin University, Kent Street, Bentley, WA 6102, Australia (corresponding author). Email: thong.pham@curtin.edu.au

[2]Senior Lecturer, School of Civil, Environmental and Mining Engineering, the University of Western Australia, 35 Stirling Highway, WA 6009, Australia. Email: mohamed.elchalakani@uwa.edu.au

[3] Associate Professor, School of Civil, Environmental and Mining Engineering, the University of Western Australia, 35 Stirling Highway, WA 6009, Australia. Email: ali.karrech@uwa.edu.au

[4]John Curtin Distinguished Professor, Center for Infrastructural Monitoring and Protection, School of Civil and Mechanical Engineering, Curtin University, Kent Street, Bentley, WA 6102, Australia; and School of Civil Engineering, Guangzhou University, China (corresponding author). Email: hong.hao@curtin.edu.au

understanding of the response of rubberized concrete under impact and improve its energy absorption. This study explored experimentally the use of rubberised concrete as a promising sustainable construction material for applications to construction of columns in buildings located in seismic active zones or subjected to terrorist attack, security bollards and rigid road side barriers.

Keywords: Rubberized concrete; Fiber Reinforced Polymer; Impact loading; High loading rate; Drop-weight test.

Introduction

Adding rubber from waste tires to conventional concrete to modify its properties has attracted an increasing attention from researchers and engineers. This use of rubber provides a sustainable way of disposing used tires which are among the largest and most problematic sources of waste (Elchalakani 2015; Elchalakani et al. 2016; Elchalakani et al. 2017). Previous studies have shown that the energy absorption of rubberized concrete is greater than that of conventional concrete (Atahan and Sevim 2008; Zheng et al. 2008; Ozbay et al. 2011). The high energy absorption capacity of rubberized concrete can be applied to structures where the energy absorption capacity is required rather than high strength, for example, roadside barriers (Topçu and Avcular 1997; Atahan and Sevim 2008; Elchalakani 2015) and pedestrian blocks (Sukontasukkul and Chaikaew 2006). Meanwhile, the compressive and tensile strengths and static modulus of elasticity of rubberized concrete decrease considerably with an increase of rubber content (Topçu 1995; Sukontasukkul and Chaikaew 2006; Elchalakani 2015). The reduction in these properties depends on many factors, such as the replacement of fine aggregates and/or coarse aggregates, the percentage of the rubber replacement, and the use of any supplementary cementitious material such as silica fume. Therefore, the gain in the energy absorption and the loss in the strength need to be compromised to provide an optimal design for a particular application. Understanding the mechanical properties of rubberized concrete under static loads is relatively more comprehensive than that under dynamic loads. There have been many studies focusing on the properties of rubberized concrete under static tests (Pacheco-Torgal et al. 2012) while the number of studies devoted to dynamic properties of rubberized concrete is limited (Liu et al. 2012).

The impact resistance of rubberized concrete has been investigated in previous studies (Topçu and Avcular 1997; Atahan and Yücel 2012; Liu et al. 2012; Gupta et al. 2015; Donga et al.

2016). It is worth mentioning that the impact resistance includes the dynamic energy absorption and strength (ACI 544.2R-17 2017). The impact resistance can be investigated by many different impact mechanisms and parameters, which are classified as weighted pendulum Charpy-type impact test, drop-weight test, constant strain-rate test, projectile impact test, split Hopkinson pressure bar test, explosive test, and instrumented pendulum impact test (ACI 544.2R-17 2017). Most of the studies in the open literature investigate the impact resistance of rubberized concrete by conducting simple drop-weight tests according to ACI 544.2R-17 (2017). The simplest method of the impact tests mentioned above is the repeated drop-weight impact test. The testing apparatus includes a 4.54 kg hammer ball dropping from 0.45 m height. The hammer ball is dropped multiple times on the specimen until the occurrence of the first crack and the ultimate failure. The energy absorption is measured from this type of impact test but not the strength. However, results of this type of impact tests vary significantly as commented by ACI 544.2R-17 (2017). More reliable testing results are sought to be used with higher confidence. Therefore, this study uses an instrumented drop-weight testing system, as described in more details in the subsequent parts, to examine the impact resistance of rubberized concrete with/without fiber reinforced polymer (FRP) confinement.

In addition, previous studies have shown that using FRP to confine conventional concrete can significantly improve its impact resistance (Shan et al. 2007; Uddin et al. 2008; Xiao and Shen 2012; Pham and Hao 2016b; Pham and Hao 2017a). The confinement effect of FRP is thus expected to increase the impact resistance of rubberized concrete as well. However, this has not been well studied and documented in the literature. The impact resistance of confined conventional concrete was investigated with different testing methods in previous studies, for example, Shan et al. (2007) used gas gun equipment and reached the strain rate ranging between 389 and 1621 s^{-1}, Uddin et al. (2008) utilized a drop-tower testing machine for impact tests, Xiao and Shen (2012) conducted impact tests by using an instrumented drop-weight test system,

and Pham and Hao (2017a) investigated the impact resistance of conventional concrete confined with different types of FRP by using an instrumented drop-weight apparatus. Although all the above studies concluded that using FRP can significantly improve the impact resistance, the failure mechanism and FRP efficiency have not been well investigated. The failure of the concrete cylinders in these studies could occur at the top end, the mid height, or the base of the specimens. Pham and Hao (2017a) conducted a detail analysis of the testing data and provided explanations on the mechanism associated with the different failure modes based on stress wave propagation, its interference, and the evolution of stress in the specimens. This characteristic is dependent on the impact velocity, material's properties and stress wave velocity which is directly calculated from the elastic modulus of the testing material. The studies about impact resistance of FRP confined conventional concrete are limited while there is no such study for rubberized concrete confined with FRP, which is the subject of this paper.

Rubberized concrete under dynamic loads

There have been two popular types of tests to investigate the dynamic characteristics of rubberized concrete including drop-weight tests and Split Hopkinson Pressure Bar (SHPB) tests. As mentioned previously, the drop-weight test includes two common types, for example, the simple drop-weight test and instrumented drop-weight test. The simple drop-weight tests were conducted by Gupta et al. (2015) to investigate the impact resistance of rubberized concrete. In that study, up to 25% replacement of rubber fiber was used in the rubberized concrete to investigate its energy absorption capability. The experimental results have shown that the impact energy absorption increases significantly with rubber fiber content. Donga et al. (2016) conducted experimental tests to investigate the impact resistance of rubberized concrete in which rubber fiber was used. The authors also concluded that using rubber fiber can significantly increase the impact resistance of concrete for both at first crack and ultimate failure

by up to 60%. Experimental results of the study by Ozbay et al. (2011) also agreed well with the above observation that the more rubber aggregates, the higher the energy absorption capacity of the rubberized concrete. Atahan and Yücel (2012) conducted instrumented drop-weight impact tests using Instron Dynatup 8250 testing machine. This testing machine is able to measure the impact velocity, energy absorption, and impact force on specimens. Aggregates in this study were replaced by rubber aggregate up to 100%. The experimental results from that study showed that rubberized concrete has lower peak impact forces and longer impact duration.

Furthermore, the SHPB technique was used by Liu et al. (2012) to investigate dynamic properties of rubberized concrete. Aggregates were replaced by rubber particles to improve the energy absorption of conventional concrete. Liu et al. (2012) found that the dynamic increase factor (DIF) of the rubberized concrete increased with a lower rate than that of conventional concrete. The experimental results showed that the DIF of rubberized concrete increased with either the rubber size or the rubber content. The authors proposed empirical models to estimate the dynamic strength of rubberized concrete from the corresponding normal strength concrete and the rubber content. An equation was also introduced to calculate the DIF of the rubberized concrete. The energy absorbing capacity of the rubberized concrete increased with the rubber content when rubber content was below 10%. However, the energy absorbing capacity of the rubberized concrete decreased when rubber content was in excess of 10%.

Apart from the material testing, experimental studies have been carried out on applications of rubberized concrete. Sukontasukkul et al. (2013) suggested using rubberized concrete as a cushion layer in bulletproof fiber reinforced concrete panels. The authors combined a soft layer (rubberized concrete) and a hard layer (steel fiber reinforced concrete) to sustain impact forces. The soft layer rubberized concrete was to absorb energy and allow less impact energy to the hard layer. Atahan and Sevim (2008) conducted an experimental study on real scale roadside

barriers made of rubberized concrete. The height, base width, top width, and length of the safety barriers were 1 m, 45 cm, 25 cm and 1 m, respectively. A 4-wheel vehicle with the weight of 500 kg was used in the impact tests. The authors concluded that the energy absorption increased with the amount of rubber in concrete. It is noted that the energy absorption here was determined as areas under the impact force versus deformation curves. In addition, another advantage of using rubberized concrete is that it reduces significantly the acceleration induced by an impact event thus eliminates injury risk to human occupants. The above studies concluded that rubberized concrete has higher energy absorption but lower static strength than the corresponding conventional concrete. To propose rubberized concrete with higher energy absorption and strength, this study uses FRP confinement since this technique has shown a significant increase in strength and energy absorption of conventional concrete.

Experimental program

Material characteristics

Three concrete mixes were designed to examine the effects of varying rubber content on the impact resistance. The conventional concrete served as a baseline had the compressive strength of 50 MPa. Aggregates of the rubberized concrete were replaced by rubber at 15% and 30%, in which conventional aggregates were replaced by two types of rubber aggregates including 2-5 mm diameter crumbed rubber and 5-7 mm diameter crumb rubbers as shown in Fig. 1. All the specimens had the ratios of cement, water and total aggregate remaining unchanged. The ratio of water to cement was 0.5 for all the mixes. Details of the mixture design of the rubberized concrete are presented in Table 1. The compressive strength of rubberized concrete was tested at 28 days according to AS 1012.9 (2014). The compressive strengths of 0%, 15%, and 30% rubberized concrete were 50.3 MPa, 25.0 MPa, and 14.4 MPa, respectively. The density of the specimens was 2271 kg/m^3, 2086 kg/m^3, and 1943 kg/m^3, respectively.

Rubber aggregates for all three mixes were soaked for 24 hours in a 10% sodium hydroxide solution (NaOH), as described by Mohammadi (2014). This allows the aggregate to absorb some water, improving cement bonding and reducing the possibility of rubber aggregate floating in the mix. After the treatment period, the rubber was drained, then soaked and rinsed three times in fresh water to neutralize the pH. When mixing the concrete, the rubber aggregates were combined with conventional aggregates and mixed for 1 minute with 10% of the required water, then add cement and mix for 1 minute. Next, a half of the remaining water was added and mixed for 1 minute. Lastly, the remaining amount of the water was added and mixed for 1 minute before adding superplasticizer and mixing for 1 minute, as described by Elchalakani (2015).

Test specimens

Rubberized concrete cylinders were cast and tested until failure under drop-weight tests. The cylinders had two sizes including 100mmx200mm and 100mmx100 mm. There are two groups of specimens including unconfined rubberized concrete and confined rubberized concrete which were wrapped with glass fiber reinforced polymer (GFRP). The previous study by Pham and Hao (2017a) have recommended that GFRP showed a better performance than carbon FRP under impact loads so that GFRP was used in this study. To ensure the crumb rubber has uniform distribution in the specimens, some specimens were cut in half for inspection. The uniform distribution of crumb rubbers in the specimens is presented in Fig. 2. Details of the specimens and testing results are presented in Table 2. Names of the rubberized concrete cylinders include three parts: the first part is Letter U (unconfined) or C (confined) stating the confinement status of the specimens. The digits behind these letters define the ratio of the diameter and height of the specimens. The second part indicates the volume content of aggregates replaced by rubber. The third part refers to drop height at which the projectile was

released. For instance, Specimen C11-15-3.0, which had the dimension of 100x100 mm^2 and 15% rubber content, was wrapped with two layers of GFRP and tested under 3 m drop height.

GFRP was bonded to the substrate of concrete by epoxy resin which had a tensile strength of 54 MPa, tensile modulus of 2.8 GPa, and 3.4% tensile elongation as reported in previous studies (Pham and Hao 2016a; Pham and Hao 2017b). The adhesive used was a mixture of epoxy resin and hardener at 5:1 ratio. Before the first GFRP layer was attached, the adhesive was spread onto the specimen's surface and GFRP was attached to the surface. After the first ring, the adhesive was spread onto the surface of the first FRP layer and the second layer was continuously bonded, ensuring that 100 mm overlap in the hoop direction was maintained. All the confined specimens in this study were wrapped with two layers of GFRP.

The GFRP was the same type from the same supplier used in a number of previous studies (Hadi et al. 2013; Pham et al. 2013; Pham et al. 2015a; Pham et al. 2015b; Pham and Hao 2016a; Pham et al. 2017; Pham and Hao 2017b). In these studies, GFRP flat coupons were fabricated and tested according to ASTM D3039 (2008) to examine the tensile properties of the fiber. The GFRP had the width of 50 mm with a unidirectional fiber density of 440 g/m^2. The nominal thickness of GFRP was 0.35 mm and the tensile strength was 833 MPa. The average strain at the maximum tensile force and the average elastic modulus were 1.97% and 41 GPa, respectively.

Test set-up

The instrumented drop-weight test for investigating the impact behavior was adopted in this study. This testing apparatus was well setup and used in the previous studies (Pham and Hao 2016a; Pham and Hao 2017b), thus only brief information is provided here. Drop-weight impact tests were conducted by dropping a steel projectile from a certain height onto the top of the

specimens, as shown in Fig. 3. The projectile was made of a solid steel cylinder, weighing 100 kg. It is worth mentioning that the shape of the projectile plays an important role to the impact force and the impact contact thus it was designed to have a smooth flat bottom with a radius r = 50 mm. To ensure the projectile falling vertically to the targets, a plastic guiding tube was utilized. A load cell was placed at the bottom of the specimens to measure the impact force. The reason to locate the load cell at the bottom of the specimens was explained in the study by Pham and Hao (2017a). A high-speed camera which was set to capture 45000 frames per second was used to monitor the failure processes, displacement, velocities, and accelerations of the projectile and the specimens. The used frame rate was set after a few trials to compromise the sampling rate and the image size. The data acquisition system controlled by a computer was used to record signals from the load cell and strain gauges. The data acquisition system recorded data at a sampling rate of 1 MHz as recommended in the previous study by Pham and Hao (2017a). In the latter study, the authors investigated the effect of different sampling rates on the recorded data and suggested that a sampling rate less than 1 MHz may not yield accurate results in this circumstance.

Experimental results

Failure mode and crack propagation

The failure modes of the unconfined and confined specimens were different. The unconfined specimens failed by splitting patterns and cracks propagated from the top downwards as shown in Fig. 4. The rubber content and the impact velocity had no effect on the failure mode of the specimens in this study. Meanwhile, the diameter-to-height ratio did show an influence on the failure mode and crack propagation as shown in Fig. 4. All the unconfined specimens had cracks propagating from the top to the bottom except Specimens U12-30-1.5 and U12-30-3.0. The crack propagation in these specimens stopped almost at mid height of the specimens. Crack

propagation in the reference specimen (U12-00-1.5 and U12-00-3.0) took approximately 1 ms and 0.7 ms to reach the bottom under 1.5 m and 3 m drop height, respectively. These results agree well with the experimental tests by Pham and Hao (2017a) in which the crack propagation from the top to the bottom of the reference specimen took place in 0.9 ms under 2 m drop height. It is observed that the rubber content slowed down the crack propagation, for example, cracks of Specimens U12-15-1.5 and U12-15-3.0 took about 1.6 ms and 1.3 ms to reach to the bottom of the specimens, respectively.

All the confined specimens under 1.5 m drop height experienced minor cracks on the FRP jacket or did not fail while other confined specimens failed under 3 m drop height as shown in Fig. 5. Specimen C11-xx-3.0 failed at the mid-height by rupture of the GFRP jacket. Specimen C12-00-3.0 experienced a minor damage of the GFRP jacket at the mid-height because the impact energy is not great enough to damage this specimen at the first blow. It is clear that the level of damage increased with the rubber content since the higher the rubber content, the larger area of GFRP rupture. Particularly, Specimen C12-30-3.0 showed a variation in the failure since it had GFRP rupture at the middle of the top half. This observation can be explained by examining the failure of the corresponding unconfined specimen (U12-30-3.0) which showed damage at the top half of the specimen while its bottom half remained undamaged. Therefore, Specimen C12-30-3.0 failed by rupturing of GFRP at the middle of the top half specimen.

Impact force time history

The impact force time histories of the unconfined specimens are presented in Fig. 6 to investigate the effect of the rubber content, the diameter-to-height ratio, and the impact velocity to the maximum impact force and the impact duration. These measurements were taken from the load cell mounted on the strong floor underneath the specimens as shown in Fig. 3. The peak impact force increased with the impact velocities. All the unconfined specimens showed

241 the impact force time histories had two major peaks following by multiple smaller peaks. The
242 maximum impact forces of the rubberized concrete specimens were almost a half of those from
243 the reference specimens. The maximum impact force of the unconfined conventional concrete
244 was about 600 kN while the corresponding force for the unconfined rubberized concrete was
245 approximately 300 kN for both rubber contents. Unfortunately, data from some specimens were
246 lost due to malfunctions of the recording devices.

247 The time histories of the impact forces of the confined specimens are presented in Fig. 7. The
248 confined specimens exhibited significantly higher maximum impact forces as compared to their
249 unconfined counterparts. The maximum impact forces of the confined conventional concrete
250 and confined rubberized concrete were 1200 kN (except for C11-00-1.5 at which the measure
251 might not be accurate) and 600 kN. It again shows that the rubberized concrete significantly
252 reduces the maximum impact forces regardless of the confinement status.

253 **Discussions on the impact resistance**

254 The impact resistance of the rubberized concrete includes four measures: the maximum impact
255 force, the impact duration, the impact impulse, and the energy absorption. The effects of the
256 rubber content, the diameter-to-height ratio, and the impact velocity on these factors will be
257 discussed in order for easy reference. Before analyzing any results from these impact tests, the
258 impact mechanism and stress wave propagation are briefly presented. This solution was
259 presented by Johnson (1972) and adopted by Pham et al. (2018) to explain the stress evolution
260 in impact tests.

261 Assuming a short cylinder made of an elastic-linear strain-hardening material sitting on a
262 frictionless flat rigid base is impacted by a rigid projectile with a speed *V*. When the projectile
263 impacts the cylinder, a stress wave propagates from the impact end downwards to the bottom
264 of the cylinder. There are two possible waves travelling at different speeds, i.e., the elastic wave

speed (c_0) and the plastic wave speed (c_1) (Johnson 1972). When impact energy is excessive to generate plastic deformation, these two waves simultaneously propagate from the impact end. The two waves travel along the cylinder at speeds of c_0 and c_1 as shown in Fig. 8b. A plastic wave, which has the stress (σ_0) is greater than the yield stress (Y), travels with the speed c_1. The elastic and plastic wave velocities can be calculated by

$$c_0 = \sqrt{\frac{E}{\rho_0}} \tag{1}$$

$$c_1 = \sqrt{\frac{P}{\rho_0}} \tag{2}$$

where E and P are respectively Young's modulus and the plastic modulus of the material, and ρ_0 is the density of the material in its unstrained state. When the elastic stress wave has arrived at the support, the material is already stressed to the compressive yield state. As a result, the reflected wave from the base must be a plastic wave as shown in Fig. 8e. The incoming plastic wave interferes with the reflected plastic wave at A. After this moment, there are only two plastic waves travelling in the material while there is no elastic wave. Johnson (1972) presented a solution to calculate stress in the specimen at any instant within $6L/c_1$ and the resulting stress is not linearly and uniformly distributed along the longitudinal axis of the cylinder. If the impact velocity is sufficiently high, the stress in Zone 2 at the impact end may reach the failure stress of the material and thus damage occurs at the impact end. Otherwise, damage may occur at the base end (Zone 3) if the material at the impact end can resist the impact. It is noted that damage rarely occurs at Zone 1 since the stress in this zone is not proportional to the impact velocity but the material properties. In general, damage occurs at a zone when the stress at that zone first reaches the failure stress of the material as shown in Fig. 8f. This stress evolution explains why the rubberized concrete damages at the top as Specimen U12-30-1.5 while other specimens with

no rubber content failed by splitting mode at which the damage occurred in the whole specimen, for example, Specimen U12-00-1.5 in Fig. 4.

Maximum impact force

The maximum impact forces of the specimens are shown in Fig. 9. As can be seen clearly from the figure that the GFRP confinement significantly increases the maximum impact forces. The maximum forces of the confined specimens are compared with their unconfined counterparts to examine the confinement efficiency. On average, the maximum impact forces of the confined specimens are equal to 2.18 their counterparts. In addition, the rubber content did show significant influence on the maximum impact force where the specimens showed a consistent reduction with increasing the rubber content. The specimens with 15% rubber content showed a reduction in the maximum impact force by about 50% as compared to the reference specimen. However, further increasing the rubber content to 30% only results in a slight decrease in the maximum impact force. The diameter-to-height ratio does not have a considerable effect on the maximum impact force except Specimen C11-00-1.5 which had the maximum impact force of 754 kN. Considering the trend of all the specimens, this number seems to be an error in measurement. Meanwhile, the impact velocity had a slight influence on the maximum impact forces at which the higher impact velocity results in higher maximum impact force. This observation agrees with the experimental testing reported by Pham and Hao (2017a). In general, rubber can be used effectively in the rubberized concrete to reduce the maximum impact force. The ability to reduce the maximum impact force of the rubberized concrete makes it a very promising applicant for roadside barriers.

Impact duration

309 The impact duration, which is traced from the load cell data, is taken to be the time period
310 between the starting point of the impact force time histories and the point at which the measured
311 force returned to zero. At this point the projectile had either rebounded or kept moving in the
312 same direction as the specimen deformation with the same velocity. In the second scenario, the
313 specimens were fully damaged and no longer carry any loads. The impact duration of all the
314 specimens is presented in Fig. 10. The GFRP confinement can significantly extend the impact
315 duration up to about 2 ms for conventional concrete and up to 4.3 ms for the rubberized
316 concrete. This characteristic is beneficial for impact resistance because longer impact durations
317 allow the stress wave to travel to a longer distance and transmit to more parts of a structure
318 which results in more global response and energy dissipation of a structure. It is worth
319 mentioning that under very short impact duration which is usually associated with great impact
320 velocity, structures commonly experience a catastrophic local damage which absorbs less
321 energy than the favorable ductile global failure mode. In the meantime, the impact velocity and
322 the diameter-to-height ratio of specimen did not have a clear influence on the impact duration.

323 ***Impact impulse***

324 The impact impulse is determined by the area under the impact force time histories of the
325 specimens as shown in Fig. 11. From this figure, it is obvious that the impact impulse of the
326 confined specimens was significantly greater than that of the unconfined counterparts. On
327 average, the impact impulses of the confined specimens increase by 6.79 times as compared to
328 those of the corresponding unconfined specimens. The impact impulse decreases with the
329 increase of the rubber content. It is more obvious for the unconfined specimens while there is
330 only a slight decrease in the impact impulses of the confined specimens. However, a number of
331 the missing data from the load cell makes it difficult to draw a conclusion on the impact impulse.

To re-examine the impact impulse of all the specimens, images from the high speed camera are used. Based on the tracking spots which were marked on the projectile, the image processing technique is adopted to calculate the velocities at the beginning and the end of an impact event. The momentum-impulse theorem is utilized to determine the change of the momentum which is equal to the impact impulse as follows:

$$I = m\Delta V = m(V_0 - V_1) = I \tag{3}$$

where m is the weight of the projectile, V_0 and V_1 are respectively the velocities of the projectile prior to the impact event and at the end of impact, and I is the impulse of the impact force. The impact impulses traced by the images of all the specimens are presented in Fig. 12. As can be seen from Figs. 11 and 12, the impact impulses calculated by two different methods agree very well with each other. These consistent results also confirm that the momentum-impulse theorem can be adopted in this circumstance with high accuracy. From Fig. 12, the experimental results again confirm that the impact impulse reduces with an increase of the rubber content and this trend in the unconfined specimens is clearer than that in the confined specimens. It is noted that this observation is different from the previous studies where it was concluded that the impact impulse increases with the rubber content (Ozbay et al. 2011; Atahan and Yücel 2012; Gupta et al. 2015; Donga et al. 2016). However, the observation and results in this study were carefully examined by two different methods which consistently show that the impact impulse decreases with an increase of the rubber content. In addition, the unclear trend of the effect of the rubber content on the impact impulse was also reported in the literature (Liu et al. 2012), where it was found that the energy absorbing capacity of the rubberized concrete increased with the rubber content when rubber contents were below 10% while it decreased when rubber content was greater than 10%. The observations can be attributed to the reduction of the impact resistance and the elongation of the impact duration with replacement of aggregates by rubber. In the

present tests the peak impact force reduced by about 50% with rubber replacement but the increment in the impact duration is not as significant. Therefore a reduced impulse is obtained from the recorded data. This difference can also be attributed to different testing techniques used in the impact tests. These different testing methods are simple drop-weight impact test (Ozbay et al. 2011; Elchalakani 2015; Gupta et al. 2015), instrumented drop-weight impact test (Atahan and Yücel 2012), and SHPB (Liu et al. 2012). Among these studies, results from the simple drop-weight impact tests vary significantly, as mentioned by ACI 544.2R-17 (2017), and thus an accurate conclusion is difficult to achieve. Meanwhile, Atahan and Yücel (2012) used instrumented drop-weight impact tests at which the impact duration was reported about 1 second for conventional concrete and up to 4 seconds for rubberized concrete which is quite long and does not agree with other studies (Shan et al. 2007; Uddin et al. 2008; Xiao and Shen 2012; Pham and Hao 2017a) where the impact duration was about 1-2 ms. As mentioned previously, Liu et al. (2012) used SHPB for the impact tests and found that the optimal value for the impact impulse occurs when the rubber content is equal to 10%. More studies, therefore, are strongly recommended to justify this discrepancy in concluding the effect of the rubber content on the impact impulse.

Energy absorption

The energy absorption of the specimens is calculated by the change of the kinetic energy of the projectile during the impact event. It is noted that the impact event was defined as the first impact only. There was a second minor impact between some specimens and the projectile after rebounding of the projectile. By adopting the energy conservation law, the energy absorption can be calculated as follows:

$$\Delta E = \frac{1}{2} m\left(V_0^2 - V_1^2\right) = E_a \quad (4)$$

where ΔE is the change of the kinetic energy during the impact event and E_a is the energy absorbed by the specimens. The results of the energy absorption are presented in Table 3 and Fig. 13. It is noted that the velocities downwards are positive while the rebound velocities are negative.

The effect of the rubber content has shown different trends for unconfined and confined rubberized concrete because they exhibited distinguished impact responses. All the unconfined specimens failed and the projectile moved forward in the same direction of the projectile velocity (positive downward), while all the confined specimens experienced rebound of the projectile. The confined specimens either partly failed or did not fail under the impact events and the projectile rebounded with velocities in the opposite direction to the impact velocity. The energy absorption of the rubberized concrete with and without FRP confinement is different from their conventional concrete counterpart.

As shown in Fig. 13, the unconfined specimens with the diameter-to-height ratio of 1:1 showed a significant reduction of the energy absorption with an increase of the rubber content. Meanwhile, this trend in the unconfined specimens with the diameter-to-height ratio of 1:2 is not clear. However, it can be concluded that the rubberized concrete has smaller energy absorption as compared to their reference counterparts. This observation is different from the previous studies (Ozbay et al. 2011; Gupta et al. 2015; Donga et al. 2016) who used the simple drop-weight impact tests. It is noted that the method to calculate the energy absorption in this study was different from that used in the simple drop-weight tests. The energy absorption reported in this study was determined from one blow while that in the previous study was estimated from the potential energy of the ball with a number of drops. The one blow impact

401 associated with excessive energy usually induces a great plastic deformation and plastic strain
402 in the specimens while the simple drop-weight tests experience both elastic and plastic
403 deformation. Also, the rubber content used in the present study is very high compared to other
404 studies. Therefore, further studies are required to clarify this difference in the energy absorption
405 of rubberized concrete with wide range of rubber content. The impact velocity had a slight
406 effect on the energy absorption of the unconfined specimens.

407 On the other hand, the GFRP confined specimens showed a significant increase in the energy
408 absorption as compared to the corresponding unconfined ones. Interestingly, the confined
409 specimens show two clear trends of the energy absorption. Firstly, the confined rubberized
410 specimens have a slightly higher energy absorption capacity than the corresponding confined
411 conventional concrete specimens, for example, Specimens C11-00-1.5, C11-15-1.5, C11-30-
412 1.5 had the energy absorption of 1163 (J), 1252 (J), 1183(J), respectively. The impact velocity
413 did change the energy absorption of the confined specimens, for example, the energy absorption
414 of the confined specimens under 3 m drop height was almost two times of that under 1.5 m drop
415 height, for example, the energy absorption of the confined specimens under 1.5 m drop height
416 (Specimens C11-xx-1.5 and C12-xx-1.5) was about 1200 J while the corresponding energy
417 absorption of the confined specimens under 3.0 m drop height (Specimens C11-xx-3.0 and C12-
418 xx-3.0) was approximately 2800 J. On the other hand, the unconfined rubberized concrete has
419 lower energy absorption capacity as compared to the unconfined conventional concrete. The
420 energy absorption reduces with the increase of the rubber content. The different efficiency of
421 the rubber content can be explained as follows. The rubber replacement significantly reduces
422 the strength of the concrete so that the rubberized concrete fails under excessive applied
423 dynamic force and cannot absorb more energy. On the other hand, when FRP is used, the
424 rubberized concrete confined with FRP can sustain a greater force and thus can absorb more
425 energy. This explanation also means that if the impact force is small so that it does not destroy

426 the specimen, the energy absorption of the rubberized concrete can be greater than the
427 corresponding conventional concrete. This is the case in the simple drop-weight tests where the
428 drop ball does not damage a specimen at the first drop. In general, it can be concluded that
429 GFRP confinement can significantly increase the energy absorption capacity and this
430 confinement technique is particularly more effective for rubberized concrete. However, the
431 energy absorption capacity of the rubberized concrete needs to be further investigated carefully
432 in conjunction with the impact damage mechanism and particular rubber content.

433 **Concluding remarks**

434 The impact tests were carried out in this study by using an instrumented drop-weight testing
435 apparatus. The experimental results in this study have shown that rubberized concrete
436 significantly reduces the maximum impact force and prolong the impact duration. These
437 characteristic make rubberized concrete a promising material for protective structures and
438 particularly for roadside barriers. The findings in this study can be summarized as:

439 1. Rubberized concrete can reduce the maximum impact force (up to 50%) and extend the
440 impact duration.

441 2. GFRP confinement is a very effective method to improve the impact resistance for
442 conventional concrete, and particularly for rubberized concrete.

443 3. The diameter-to-height ratio affected the failure modes and damage propagation. It had a
444 slight to moderate effect on the impact resistance including the impact force, the impact
445 duration, and the impact impulse.

446 4. The unconfined rubberized concrete has a lower energy absorption capacity as compared
447 to conventional concrete under excessive impact energy. However, from sustainability

point of view, recycling great amount of rubber in a concrete roadside barrier for example, may lead to a design compromise for better structure and passenger protection.

5. The rubberized concrete reduces the maximum impact force so that it transfers lower force to a protected structure as well as lower rebound force in the case of roadside barriers. However, further research is needed to provide more understanding about this topic and special attention should be paid to examining the impact energy absorption associated with the impact damage mechanism for a wide range of rubber contents.

6. The preliminary results of this study of rubberized concrete with or without GFRP confinement are promising for application of such materials in designing protective structures.

Acknowledgements

The authors would like to deeply thank Liam O'keefe from Tyres Stewardship Australia and Adrian Jones from Tyrecycle. Thanks are given to Andrew Sarkady and Anup Chakrabortty from BASF for kindly donating the superplasticizer required for all the specimens. Thanks are given to the following technicians Matt Arpin, Malcolm Stafford, Jim Waters and Brad Rose for assisting the students in performing the experiments. Thanks are given to Cameron Marshal and Armin Hosseini, David Pegrum and Aarin Ryan, former students of the University of Western Australia for performing the tests and processing the test data.

References

ACI 544.2R-17 (2017). "Report on the Measurement of Fresh State Properties and Fiber Dispersion of Fiber-Reinforced Concrete." American Concrete Institute, Farmington Hills, MI.

AS 1012.9 (2014). "Compressive strength tests - concrete." *1012.9: 2014*Sydney, NSW, Australia.

ASTM D3039 (2008). "Standard Test Method for Tensile Properties of Polymer Matrix Composite Materials." *D3039:2008*West Conshohocken, PA.

Atahan, A. O., and Sevim, U. K. (2008). "Testing and comparison of concrete barriers containing shredded waste tire chips." *Materials Letters*, 62(21), 3754-3757.
Atahan, A. O., and Yücel, A. Ö. (2012). "Crumb rubber in concrete: Static and dynamic evaluation." *Construction and Building Materials*, 36, 617-622.
Donga, P. D., Shah, D., and Bhavsar, J. K. (2016). "Impact Resistance of Waste Rubber Fiber Silica Fume Concrete." *Journal of Civil Engineering and Environmental Technology*, 3(4), 274-279.
Elchalakani, M. (2015). "High strength rubberized concrete containing silica fume for the construction of sustainable road side barriers." *Structures*, 1, 20-38.
Elchalakani, M., Aly, T., and Abu-Aisheh, E. (2016). "Mechanical properties of rubberised concrete for road side barriers." *Australian Journal of Civil Engineering*, 14(1), 1-12.
Elchalakani, M., Basarir, H., and Karrech, A. (2017). "Green Concrete with High-Volume Fly Ash and Slag with Recycled Aggregate and Recycled Water to Build Future Sustainable Cities." *Journal of Materials in Civil Engineering*, 29(2).
Gupta, T., Sharma, R. K., and Chaudhary, S. (2015). "Impact resistance of concrete containing waste rubber fiber and silica fume." *International Journal of Impact Engineering*, 83, 76-87.
Hadi, M. N. S., Pham, T. M., and Lei, X. (2013). "New method of strengthening reinforced concrete square columns by circularizing and wrapping with fiber-reinforced polymer or steel straps." *Journal of Composites for Construction*, 17(2), 229-238.
Johnson, W. (1972). *Impact strength of materials*, Edward Arnold London.
Liu, F., Chen, G., Li, L., and Guo, Y. (2012). "Study of impact performance of rubber reinforced concrete." *Construction and Building Materials*, 36, 604-616.
Mohammadi, I. (2014). "Investigation on the use of crumb rubber concrete (CRC) for rigid pavements."
Ozbay, E., Lachemi, M., and Sevim, U. K. (2011). "Compressive strength, abrasion resistance and energy absorption capacity of rubberized concretes with and without slag." *Materials and Structures*, 44(7), 1297-1307.
Pacheco-Torgal, F., Ding, Y., and Jalali, S. (2012). "Properties and durability of concrete containing polymeric wastes (tyre rubber and polyethylene terephthalate bottles): An overview." *Construction and Building Materials*, 30, 714-724.
Pham, T. M., Doan, L. V., and Hadi, M. N. S. (2013). "Strengthening square reinforced concrete columns by circularisation and FRP confinement." *Construction and Building Materials*, 49, 490-499.
Pham, T. M., Hadi, M. N. S., and Tran, T. M. (2015a). "Maximum usable strain of FRP-confined concrete." *Construction and Building Materials*, 83, 119-127.
Pham, T. M., Hadi, M. N. S., and Youssef, J. (2015b). "Optimized FRP wrapping schemes for circular concrete columns." *Journal of Composites for Construction*, 19(6), 04015015.
Pham, T. M., and Hao, H. (2016a). "Impact behavior of FRP-strengthened RC beams without stirrups." *Journal of Composites for Construction*, 20(4), 04016011.
Pham, T. M., and Hao, H. (2016b). "Review of concrete structures strengthened with FRP against impact loads." *Structures*, 7, 59-70.
Pham, T. M., Hadi, M. N. S., and Youssef, J. (2017). "Effects of fabrication technique on tensile properties of fiber reinforced polymer." *Journal of Testing and Evaluation*, 45(5), 1-11.
Pham, T. M., and Hao, H. (2017a). "Axial impact resistance of FRP-confined concrete." *Journal of Composites for Construction*, 21(2), 04016088.
Pham, T. M., and Hao, H. (2017b). "Behavior of fiber reinforced polymer strengthened reinforced concrete beams under static and impact loads." *International Journal of Protective Structures*, 8(1), 1-22.

Pham, T. M., Chen, W., and Hao, H. (2018). "Failure and impact resistance analysis of plain and FRP-confined concrete cylinders under axial impact loads." *International Journal of Protective Structures*, 9(1), 4-23.

Shan, J. H., Chen, R., Zhang, W. X., Xiao, Y., and Lu, F. Y. (2007). "Behavior of Concrete Filled Tubes and Confined Concrete Filled Tubes under High Speed Impact." *Advances in Structural Engineering*, 10(2), 209-218.

Sukontasukkul, P., and Chaikaew, C. (2006). "Properties of concrete pedestrian block mixed with crumb rubber." *Construction and Building Materials*, 20(7), 450-457.

Sukontasukkul, P., Jamnam, S., Rodsin, K., and Banthia, N. (2013). "Use of rubberized concrete as a cushion layer in bulletproof fiber reinforced concrete panels." *Construction and Building Materials*, 41, 801-811.

Topçu, I. B. (1995). "The properties of rubberized concretes." *Cement and Concrete Research*, 25(2), 304-310.

Topçu, I. B., and Avcular, N. (1997). "Collision behaviours of rubberized concrete." *Cement and Concrete Research*, 27(12), 1893-1898.

Uddin, N., Purdue, J. D., and Vaidya, U. (2008). "Feasibility of thermoplastic composite jackets for bridge impact protection." *Journal of Aerospace Engineering*, 21(4), 259-265.

Xiao, Y., and Shen, Y. (2012). "Impact Behaviors of CFT and CFRP Confined CFT Stub Columns." *Journal of Composites for Construction*, 16(6), 662-670.

Zheng, L., Sharon Huo, X., and Yuan, Y. (2008). "Experimental investigation on dynamic properties of rubberized concrete." *Construction and Building Materials*, 22(5), 939-947.

546 **List of Figures**

List of Tables

564 Table 1. Mixture design of rubberized concrete

Specimens	Fine aggregate (0-5 mm) (kg/m^3)	Coarse aggregate (5-7 mm) (kg/m^3)	Rubber aggregates (2-7 mm) (kg/m^3)	Water (kg/m^3)
0% rubber	973	750	0	213
15% rubber	827	638	112	213
30% rubber	681	525	224	213

565

566 Table 2. Test matrix and experimental results

Group	Specimen	Drop height (m)	Rubber content (%)	Peak Impact force (kN)	Impact duration (ms)	Impulse (kN.ms)
Unconfined specimens	U11-00-1.5	1.5	0	-	-	-
	U11-00-3.0	3.0		616	0.566	202
	U11-15-1.5	1.5	15	193	1.646	163
	U11-15-3.0	3.0		320	0.790	115
	U11-30-1.5	1.5	30	209	0.835	81
	U11-30-3.0	3.0		219	0.902	79
	U12-00-1.5	1.5	0	-	-	-
	U12-00-3.0	3.0		661	0.660	174
	U12-15-1.5	1.5	15	-	-	-
	U12-15-3.0	3.0		346	0.858	127
	U12-30-1.5	1.5	30	230	0.872	93
	U12-30-3.0	3.0		-	-	-
Confined specimens	C11-00-1.5	1.5	0	754	1.962	794
	C11-00-3.0	3.0		1154	2.039	1039
	C11-15-1.5	1.5	15	630	2.256	758
	C11-15-3.0	3.0		612	4.285	858
	C11-30-1.5	1.5	30	455	3.348	752
	C11-30-3.0	3.0		547	1.598	428
	C12-00-1.5	1.5	0	1081	2.014	805
	C12-00-3.0	3.0		1158	2.014	1039
	C12-15-1.5	1.5	15	523	2.880	758
	C12-15-3.0	3.0		680	3.201	1045
	C12-30-1.5	1.5	30	462	3.535	760
	C12-30-3.0	3.0		527	3.588	826

567 - Lost data due to malfunction in the acquisition system
568

569 Table 3. Energy absorption of the tested specimens

Group	Specimen	Drop height (m)	Rubber content (%)	Impact velocity (m/s)	Residual velocity (m/s)	Energy absorption (J)
Unconfined specimens	U11-00-1.5	1.5	0	5.43	2.49	1163
	U11-15-1.5		15	5.47	2.21	1252
	U11-30-1.5		30	5.38	2.31	1183
	U11-00-3.0	3.0	0	7.72	2.09	2762
	U11-15-3.0		15	7.88	1.33	3015
	U11-30-3.0		30	7.73	1.59	2864
	U12-00-1.5	1.5	0	5.60	2.20	1322
	U12-15-1.5		15	5.57	2.24	1303
	U12-30-1.5		30	5.58	1.39	1460
	U12-00-3.0	3.0	0	7.90	2.31	2855
	U12-15-3.0		15	7.85	2.53	2763
	U12-30-3.0		30	7.71	0.12	2974
Confined specimens	C11-00-1.5	1.5	0	5.47	-2.53	1178
	C11-15-1.5		15	5.39	-3.34	894
	C11-30-1.5		30	5.48	-4.45	512
	C11-00-3.0	3.0	0	7.73	-5.28	1592
	C11-15-3.0		15	7.87	-6.03	1279
	C11-30-3.0		30	7.84	-6.30	1093
	C12-00-1.5	1.5	0	5.65	-3.21	1082
	C12-15-1.5		15	5.57	-4.00	750
	C12-30-1.5		30	5.62	-3.76	869
	C12-00-3.0	3.0	0	7.96	-6.50	1056
	C12-15-3.0		15	7.90	-6.23	1183
	C12-30-3.0		30	7.79	-6.67	810

570

571

572

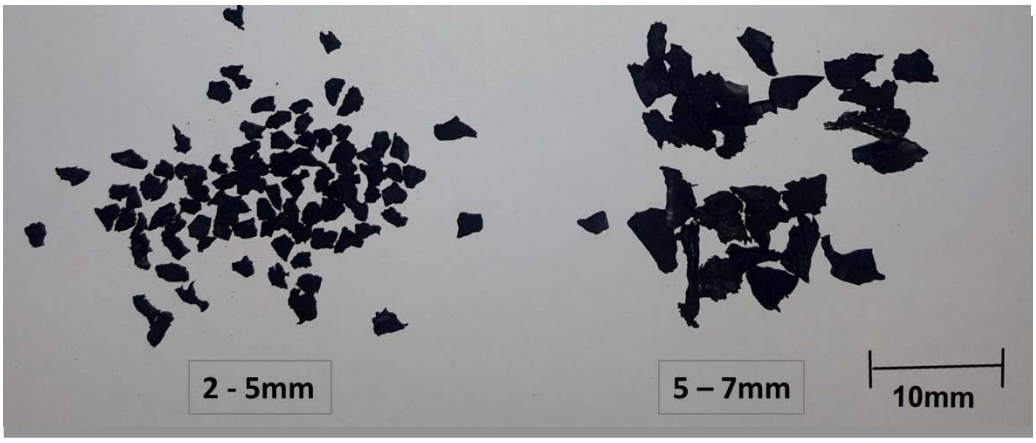

573 Fig. 1. Rubber aggregates

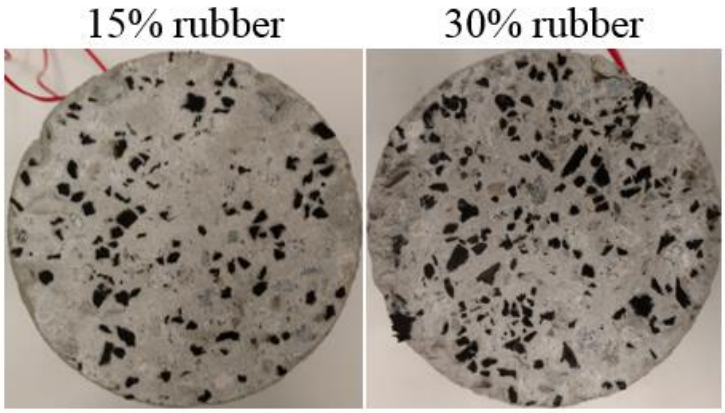

574

575 Fig. 2. Distribution of rubber in the specimens

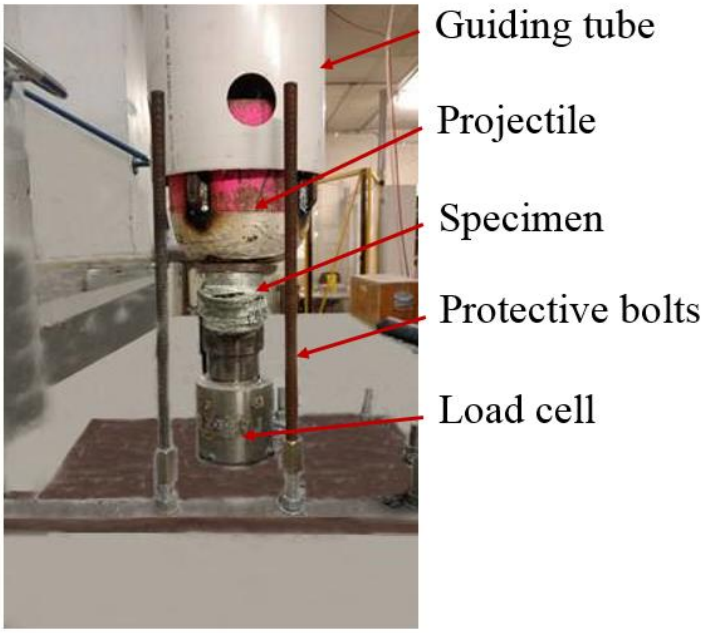

576

577 Fig. 3. Drop-weight test apparatus

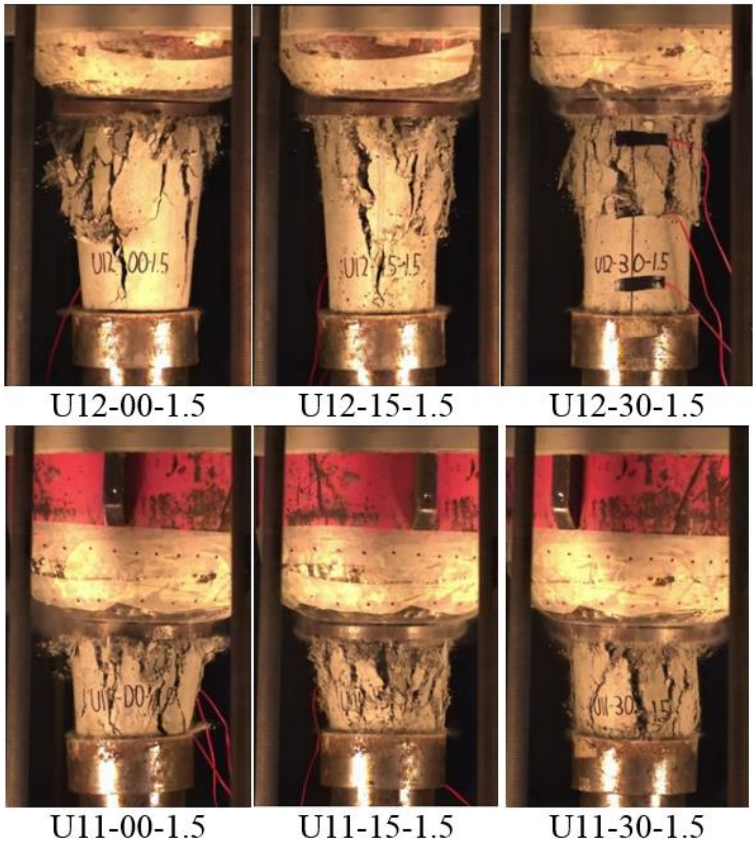

578

579 Fig. 4. Failure of the unconfined specimens (1.5 m drop height)

580

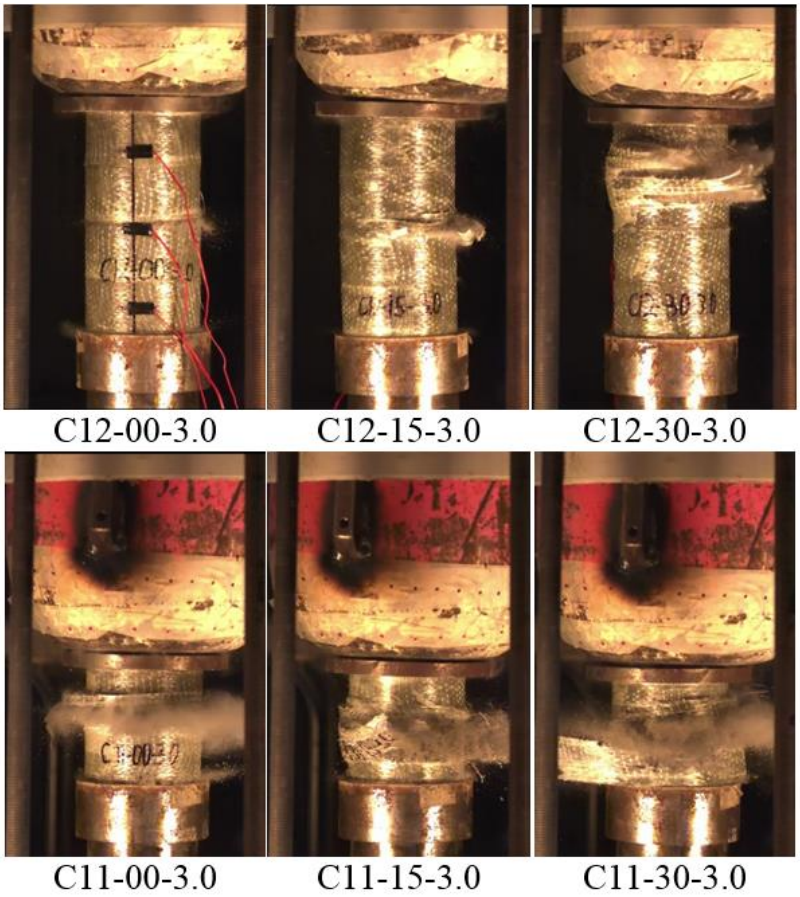

Fig. 5. Failure of the confined specimens (3 m drop height)

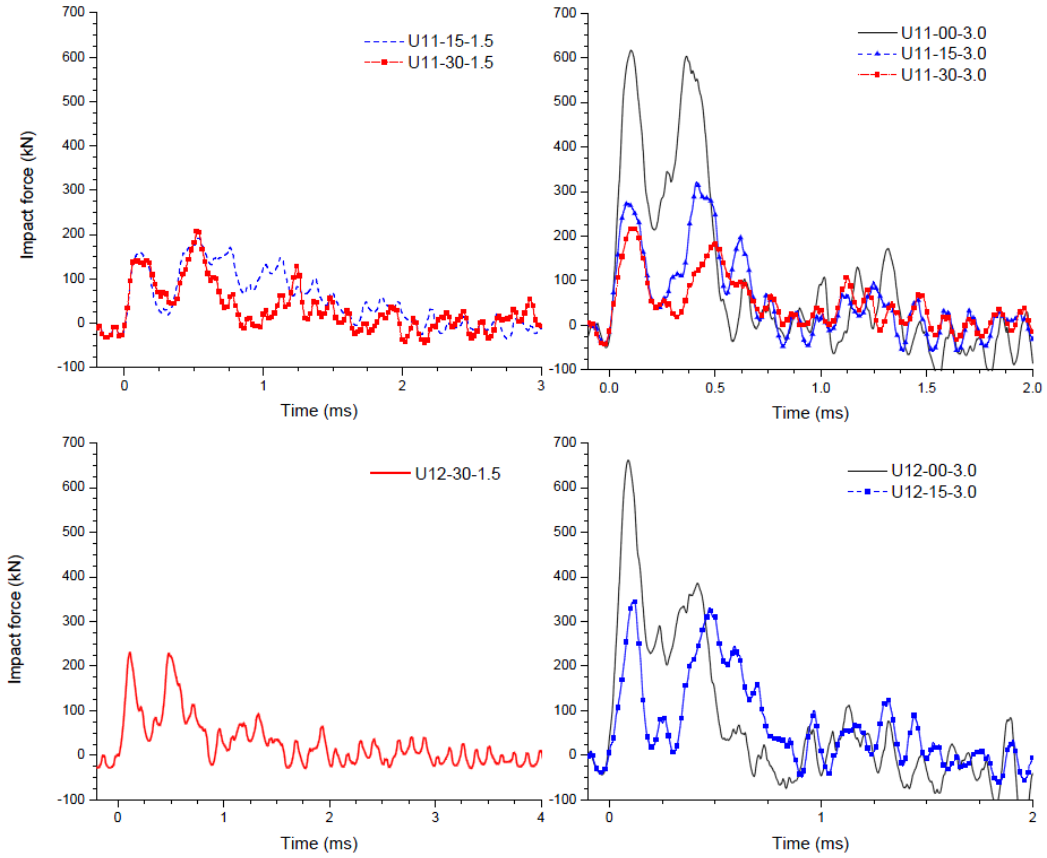

584

585 Fig. 6. Impact force time histories of unconfined specimens

586

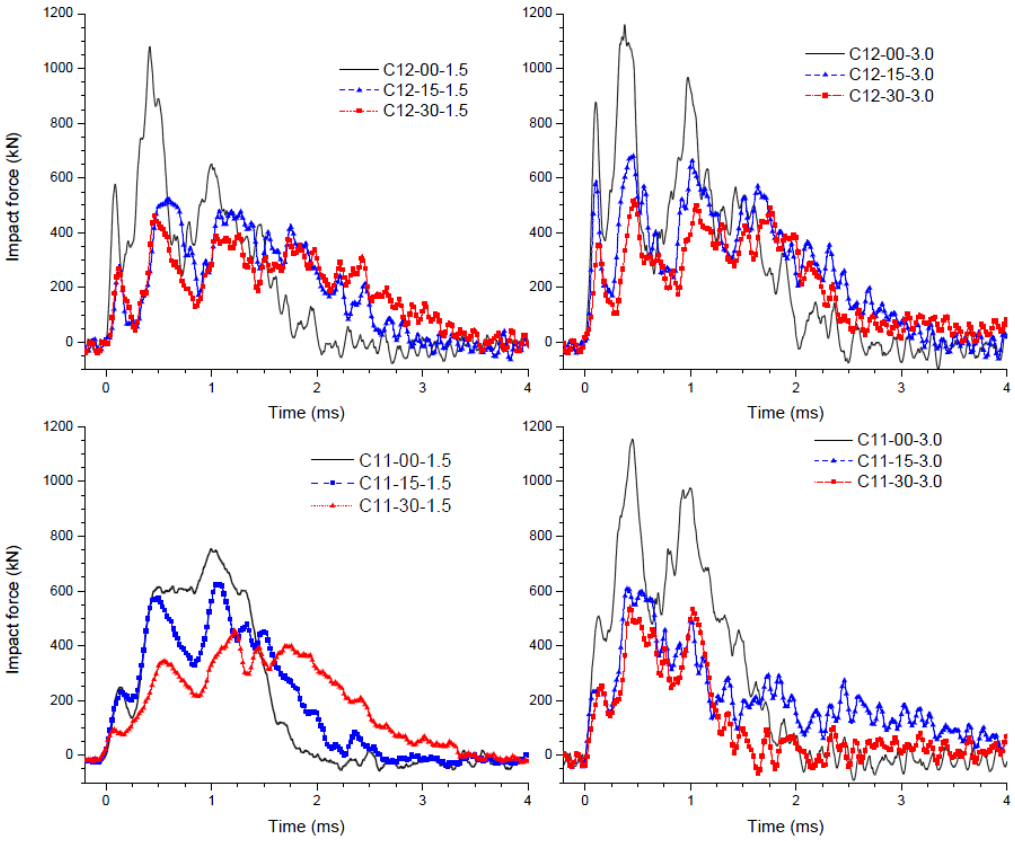

587

588 Fig. 7. Impact force time histories of confined specimens

589

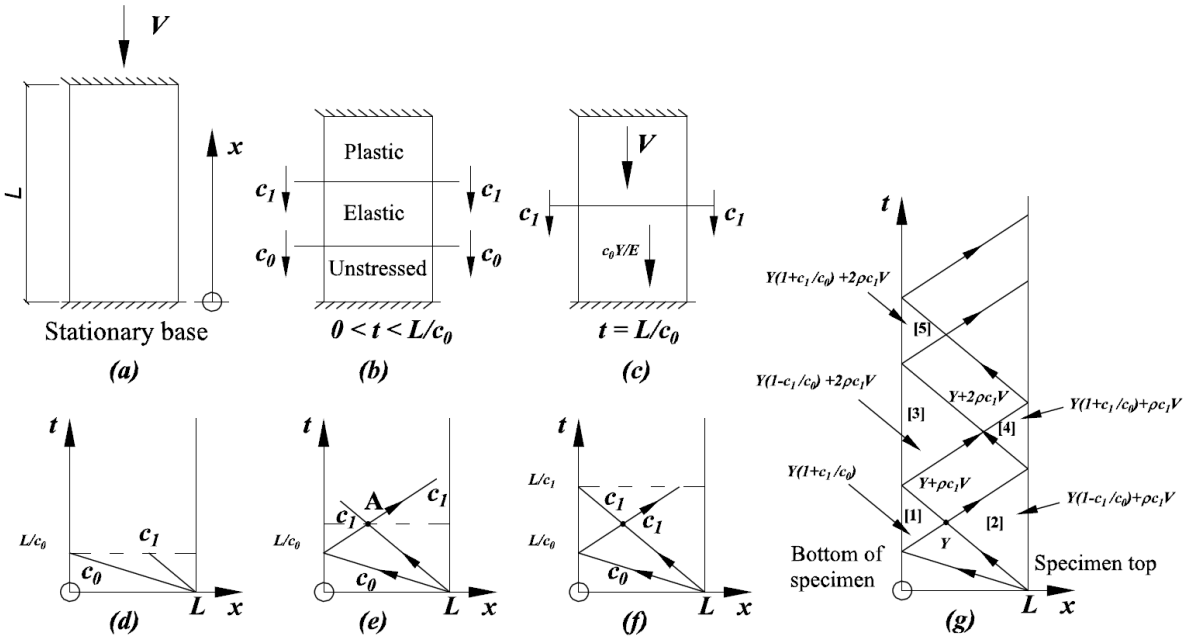

Figure 8. Stress evolution mechanism under impact

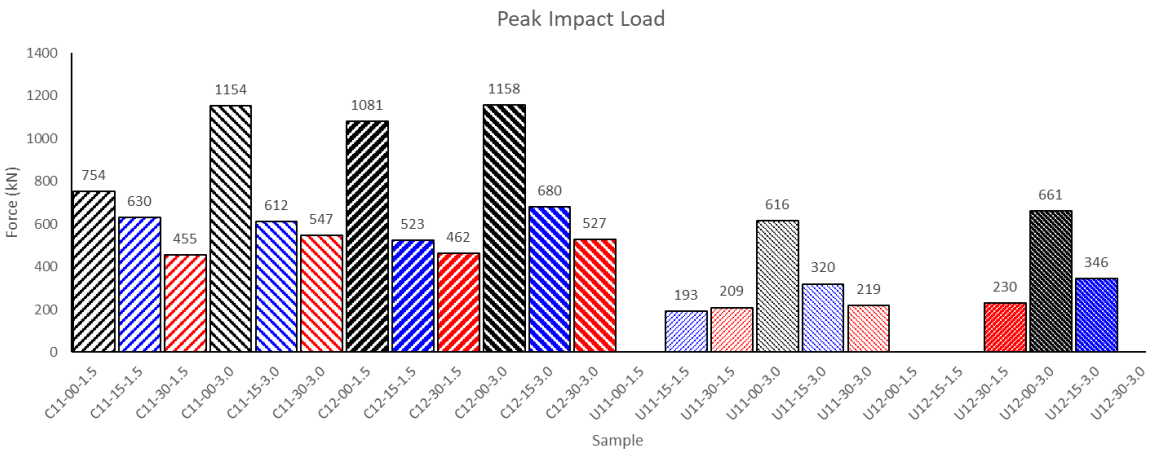

593

594 Figure 9. Maximum impact forces of the tested specimens

595

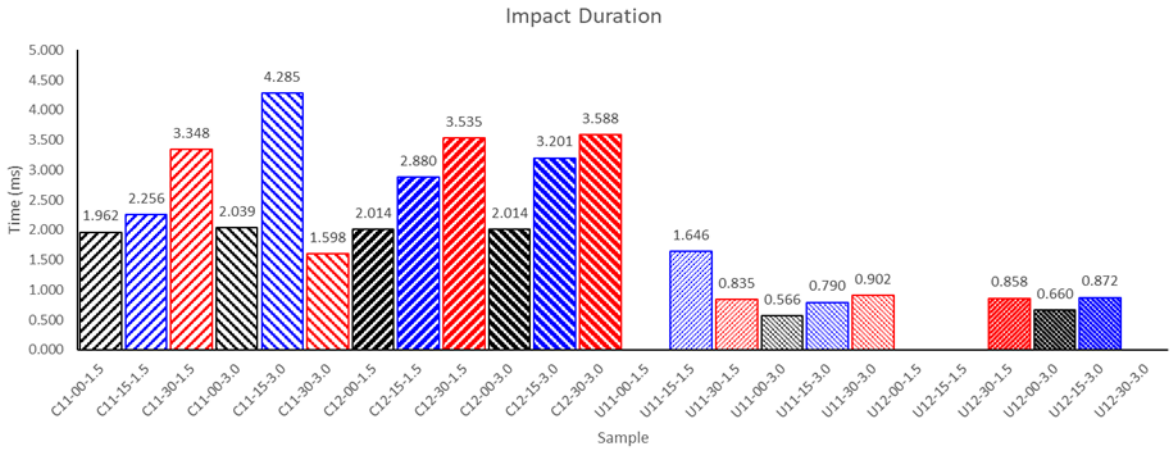

596

597 Figure 10. Impact duration of the tested specimens

598

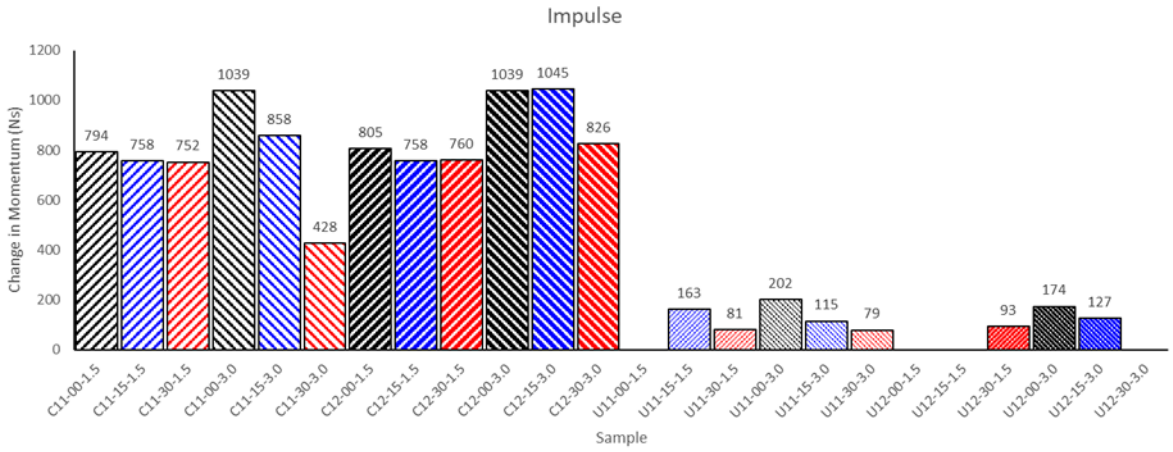

599

600 Figure 11. Impact impulse of the tested specimens (load cell data)

601

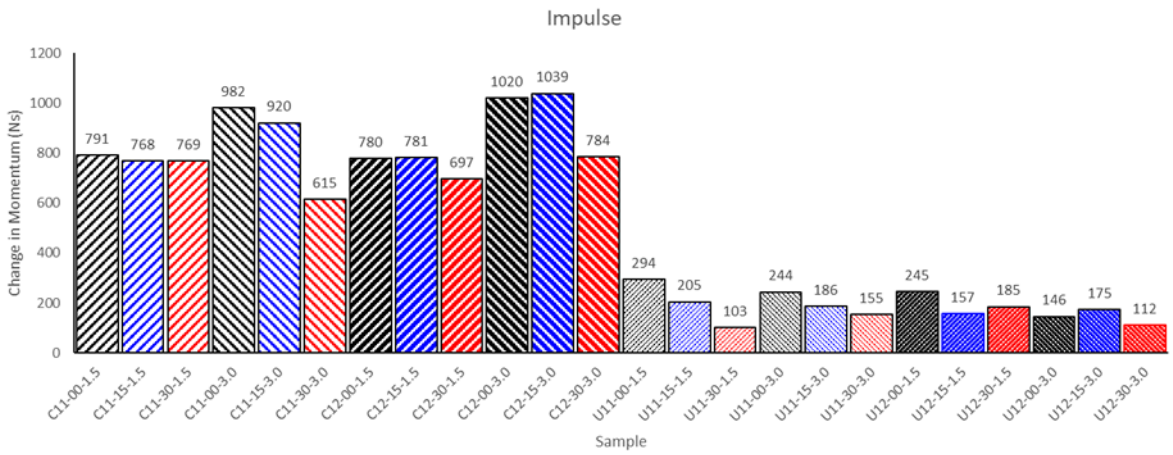

602

603 Figure 12. Impact impulse of the tested specimens (from image processing)

604

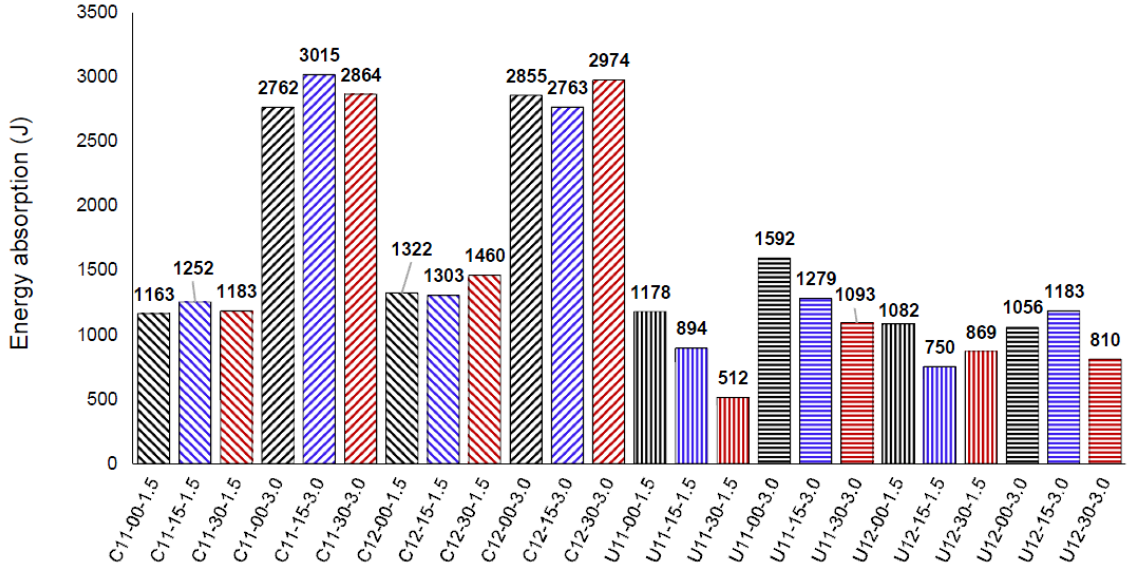

Figure 13. Energy absorption of the tested specimens (data from images processing)